



# Impacts of snowpack emissions on deduced levels of OH and peroxy radicals at Summit, Greenland

J. Yang<sup>a</sup>, R.E. Honrath<sup>a,\*</sup>, M.C. Peterson<sup>a</sup>, J.E. Dibb<sup>b</sup>, A.L. Sumner<sup>c</sup>,  
P.B. Shepson<sup>c</sup>, M. Frey<sup>d</sup>, H.-W. Jacobi<sup>d</sup>, A. Swanson<sup>e</sup>, N. Blake<sup>e</sup>

<sup>a</sup>Department of Civil and Environmental Engineering, Michigan Technological University, 1400 Townsend Dr. Houghton, MI 49931-1295, USA

<sup>b</sup>Climate Change Research Center, University of New Hampshire, Durham, USA

<sup>c</sup>Departments of Chemistry, and Earth and Atmospheric Science, Purdue University, Indiana, USA

<sup>d</sup>Department of Hydrology and Water Resources, University of Arizona, USA

<sup>e</sup>Department of Chemistry, University of California, Irvine, USA

Received 4 June 2001; received in revised form 1 October 2001; accepted 11 January 2002

## Abstract

Levels of OH and peroxy radicals in the atmospheric boundary layer at Summit, Greenland, a location surrounded by snow from which HO<sub>x</sub> radical precursors are known to be emitted, were deduced using steady-state analyses applied to (OH + HO<sub>2</sub> + CH<sub>3</sub>O<sub>2</sub>), (OH + HO<sub>2</sub>), and OH–HO<sub>2</sub> cycling. The results indicate that HO<sub>x</sub> levels at Summit are significantly increased over those that would result from O<sub>3</sub> photolysis alone, as a result of elevated concentrations of HONO, HCHO, H<sub>2</sub>O<sub>2</sub>, and other compounds. Estimated midday levels of (HO<sub>2</sub> + CH<sub>3</sub>O<sub>2</sub>) reached 30–40 pptv during two summer seasons. Calculated OH concentrations averaged between 05:00 and 20:00 (or 21:00) exceeded 4 × 10<sup>6</sup> molecules cm<sup>-3</sup>, comparable to (or higher than) levels expected in the tropical marine boundary layer. These findings imply rapid photochemical cycling within the boundary layer at Summit, as well as in the upper pore spaces of the surface snowpack. The photolysis rate constants and OH levels calculated here imply that gas-phase photochemistry plays a significant role in the budgets of NO<sub>x</sub>, HCHO, H<sub>2</sub>O<sub>2</sub>, HONO, and O<sub>3</sub>, compounds that are also directly affected by processes within the snowpack. © 2002 Elsevier Science Ltd. All rights reserved.

**Keywords:** HO<sub>x</sub>; Oxidants; Steady-state model; Arctic boundary layer; Ice photochemistry

## 1. Introduction

A series of studies over the past several years have demonstrated that processes within surface snowpacks result in the release (and in some cases, the uptake) of a variety of photochemically active compounds. It appears that these effects are largely driven by three processes: photodissociation of nitrate ion present within the surface layer of ice crystals in the snowpack (Honrath et al., 2000), temperature-dependent adsorption or cocondensation onto, and desorption from, ice surfaces

(e.g. Bales et al., 1995), and autocatalytic release of halogen compounds, resulting from reactions on ice surfaces (Tang and McConnell, 1996). (The latter process has been clearly documented only near the marine boundary layer and is not considered in detail here.)

It is likely that these processes significantly alter levels of HO<sub>x</sub> (OH + HO<sub>2</sub>) in the atmospheric boundary layer above snowpacks. Photodissociation of nitrate ion near the surface of ice crystals is believed to be the source of NO<sub>x</sub> release observed from sunlight-irradiated snow (e.g. Honrath et al., 1999), and, if so, results in the production of OH radicals at the site of photodissociation. The fate of this OH is not known, but in the

\*Corresponding author.

E-mail address: reh@mtu.edu (R.E. Honrath).

presence of ubiquitous organic matter, it may result in the production and release of photolabile oxidized compounds, such as formaldehyde (Sumner and Shepson, 1999). In addition, there is direct evidence of impacts of snowpack emissions on ambient atmospheric concentrations of a variety of compounds that play direct roles in the budgets of HO<sub>x</sub> compounds. These compounds include HONO (Zhou et al., 2001; Dibb et al., 2002) and H<sub>2</sub>O<sub>2</sub> (Jacobi et al., 2002) (OH sources), HCHO (Sumner and Shepson, 1999; Jacobi et al., 2002) (an HO<sub>2</sub> source), and NO<sub>x</sub> (Ridley et al., 2000; Davis et al., 2001; Honrath et al., 2002) (which largely determines the partitioning of HO<sub>x</sub>). Recent measurements at the South Pole, which indicate that OH concentrations are higher than expected (Mauldin et al., 2001), are consistent with the expectation that the net result of these impacts is likely to increase atmospheric OH concentrations.

As part of a series of studies designed to determine the impact of snowpack photochemistry upon atmospheric and snow composition, measurements of nitrogen oxides and other species were made during two summer field seasons at Summit, Greenland (38.4°E, 72.55°N, 3200 m altitude), a site surrounded by snow for > 350 km in all directions. In this work, we analyze these measurements to deduce atmospheric levels of peroxy radicals (PO<sub>2</sub>, which in this analysis includes HO<sub>2</sub> and CH<sub>3</sub>O<sub>2</sub>) and OH at Summit during the summers of 1999 and 2000. Our goal is to quantify the magnitude of PO<sub>2</sub> and OH levels at Summit and to investigate the dominant gas-phase processes in their budgets. In particular, measurements of each of the important OH precursor compounds were made, allowing us to quantify their relative importance to the OH budget. We do not directly relate PO<sub>2</sub> and OH levels to snowpack emissions of their precursors in this paper. However, companion papers in this issue present measurements of the vertical fluxes of some of the precursor compounds above the Summit snowpack (Honrath et al., 2002; Jacobi et al., 2002).

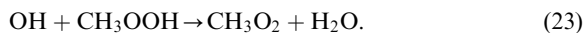
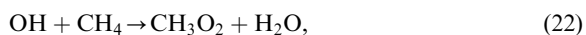
## 2. Methods

PO<sub>2</sub> and OH concentrations were estimated using steady-state analyses. This technique makes use of the fact that the daytime rates of formation and destruction of short-lived radicals are rapid, relative to the rates of change of radical concentrations, as is the rate of cycling among members of rapidly cycling radical families. Steady state was applied in three ways. First, the partitioning of HO<sub>x</sub> between OH and HO<sub>2</sub> was calculated by setting the reactions interconverting these two compounds at steady-state. Second, the total concentration of (HO<sub>x</sub> plus CH<sub>3</sub>O<sub>2</sub>) (referred to as CHO<sub>x</sub>) was determined by setting the sources and sinks of this compound group equal to one another. Finally,

the steady-state of OH was assessed. In this analysis, we have not calculated the partitioning of peroxy radicals between HO<sub>2</sub> and CH<sub>3</sub>O<sub>2</sub>, but rather set the ratio  $\alpha = [\text{HO}_2]/[\text{PO}_2]$ . The true value of  $\alpha$  at boundary layer sites (and at Summit in particular) is not well known. We have conducted simulations with  $\alpha$  varying from 0.5 to 0.9, spanning the range deduced in some previous steady-state modeling analyses (e.g. Cantrell et al., 1997; Zanis et al., 1999). The choice of  $\alpha$  affects the self-consistency of the results, as indicated by the balance of OH and HO<sub>x</sub> formation and destruction rates; this is discussed in Section 3.3.

Table 1 presents the reactions used in each steady-state analysis. The ratio [OH]/[HO<sub>2</sub>] was calculated by setting the total rate of reactions converting OH to HO<sub>2</sub> (reactions (1)–(5)) equal to total rate of reactions converting HO<sub>2</sub> to OH (reactions (6) and (7)). The concentration of PO<sub>2</sub> was then determined by setting the total rate of formation of CHO<sub>x</sub> (due to reactions (9)–(14)) equal to the total rate of CHO<sub>x</sub> destruction (via reactions (15)–(21)).

This method necessarily results in equality between the rates of formation and destruction of CHO<sub>x</sub>. It does not, however, need to result in equal rates of formation and destruction of other radical families. The rates of formation and destruction of HO<sub>x</sub> and OH were therefore also calculated. The rate of HO<sub>x</sub> formation is calculated from the same set of reactions used for CHO<sub>x</sub>, with the exception that reactions (14) and (16) produce and destroy, respectively, only one HO<sub>x</sub> (rather than two CHO<sub>x</sub>), and reaction (17) does not remove HO<sub>x</sub>. Similarly, the rate of OH formation was determined from reactions (6), (7), and (9)–(12), and the rate of OH destruction was determined from reactions (1)–(5) and (18)–(21), plus two additional reactions:



### 2.1. Measurement techniques

NO and NO<sub>2</sub> were determined as described by Honrath et al. (2002), using measurements at heights of 80–95 cm in 1999 and of 47 and 200 cm in 2000. NO and NO<sub>2</sub> measurements were obtained every ~7 min; the calculations presented below were conducted at the times of these measurements.

O<sub>3</sub> was determined each minute at the same heights as NO<sub>x</sub>, using commercial ultraviolet absorbance instruments, with different instruments used during 1999 and 2000. The instrument used during 2000 was compared to a NIST-traceable instrument at the NOAA CMDL laboratory, and agreed within 4% (S. Oltmans, NOAA CMDL, personal communication, 2001). Based on an

Table 1  
Reactions used in the steady-state analyses

OH ⇌ HO <sub>2</sub> Cycling	
OH → HO <sub>2</sub> reactions:	
OH + CO $\xrightarrow{O_3}$ HO <sub>2</sub> + CO <sub>2</sub>	(1)
OH + O <sub>3</sub> → HO <sub>2</sub> + O <sub>2</sub>	(2)
OH + HCHO $\xrightarrow{O_3}$ HO <sub>2</sub> + H <sub>2</sub> O + CO	(3)
OH + H <sub>2</sub> O <sub>2</sub> → HO <sub>2</sub> + H <sub>2</sub> O	(4)
OH + H <sub>2</sub> $\xrightarrow{O_3}$ HO <sub>2</sub> + H <sub>2</sub> O	(5)
HO <sub>2</sub> → OH reactions :	
HO <sub>2</sub> + NO → OH + NO <sub>2</sub>	(6)
HO <sub>2</sub> + O <sub>3</sub> → OH + 2O <sub>2</sub>	(7)
CHO <sub>x</sub> (HO <sub>2</sub> + OH + CH <sub>3</sub> O <sub>2</sub> ) Steady-state Sources:	
O <sub>3</sub> + <i>hν</i> → O <sub>2</sub> + O( <sup>1</sup> D) (+0)	(8)
O( <sup>1</sup> D) + H <sub>2</sub> O → 2OH (+2)	(9)
HONO + <i>hν</i> → OH + NO (+1)	(10)
H <sub>2</sub> O <sub>2</sub> + <i>hν</i> → 2OH (+2)	(11)
CH <sub>3</sub> OOH + <i>hν</i> $\xrightarrow{O_3}$ OH + HO <sub>2</sub> + HCHO (+2)	(12)
HCHO + <i>hν</i> $\xrightarrow{O_3}$ 2HO <sub>2</sub> + CO (+2)	(13)
CH <sub>3</sub> CHO + <i>hν</i> → CH <sub>3</sub> O <sub>2</sub> + HO <sub>2</sub> + CO (+2)	(14)
Sinks:	
HO <sub>2</sub> + HO <sub>2</sub> → H <sub>2</sub> O <sub>2</sub> + O <sub>2</sub> (−2)	(15)
HO <sub>2</sub> + CH <sub>3</sub> O <sub>2</sub> → CH <sub>3</sub> OOH + O <sub>2</sub> (−2)	(16)
CH <sub>3</sub> O <sub>2</sub> + CH <sub>3</sub> O <sub>2</sub> → products (−2)	(17)
OH + HO <sub>2</sub> → H <sub>2</sub> O + O <sub>2</sub> (−2)	(18)
OH + NO <sub>2</sub> $\xrightarrow{M}$ HNO <sub>3</sub> (−1)	(19)
OH + NO $\xrightarrow{M}$ HONO (−1)	(20)
OH + CH <sub>3</sub> CHO → CH <sub>3</sub> CO + H <sub>2</sub> O (−1)	(21)

intercomparison with this instrument, the instrument used during 1999 was determined to be biased low by 20%, and the 1999 measurements were therefore adjusted by the factor 1.25.

Nitrous acid was sampled at a height of ~1 m (1999) and 80 cm (with occasional measurements at heights of 200 and 400 cm) (2000) using mist chambers, and was analyzed as nitrite using ion chromatography, using methods described previously for HNO<sub>3</sub> (Dibb et al., 1998) and discussed by Dibb et al. (2002). These samples

reflect average concentrations over 24- to 38-min measurement periods. A small number (5 observations; 2% of the total number) of unusually high HONO mixing ratios which exceeded the mean of the remaining data by more than four standard deviations were removed from the 1999 dataset; none were removed from the 2000 dataset. HONO measurements from mist chamber samples that overlapped the NO<sub>x</sub> measurement times were used in calculations; NO<sub>x</sub> measurements with no overlapping mist chamber sample were excluded from calculations.

Formaldehyde was determined during 1999 at a height of 1 m using a modified version of the fluorometric method described by Fan and Dasgupta (1994). During 2000, the methods described by Jacobi et al. (2002) were used, and measurements were at heights of 143 and 152 cm. HCHO measurements were interpolated to the NO<sub>x</sub> measurement times; periods when the interpolation would have exceeded 1 h were excluded from calculations.

Hydrogen peroxide was determined using the methods described by Jacobi et al. (2002). Measurement heights during 1999 were 60–100 cm; during 2000, H<sub>2</sub>O<sub>2</sub> was determined at the same heights at HCHO. H<sub>2</sub>O<sub>2</sub> was interpolated in the same manner as HCHO.

CH<sub>4</sub>, non-methane hydrocarbons, and (in 2000) CO were determined in ambient-air canister samples taken ~1–6 times each day and analyzed using gas chromatography with flame ionization detection (GC/FID) (Blake and Rowland, 1986; Hurst, 1990; Swanson et al., 2002). CO and CH<sub>4</sub> levels were relatively constant; average values were used for each season (with the exception that 1999 CO was estimated from previous high latitude observations; Novelli, 1998). Non-methane hydrocarbons were determined to be insignificant as OH sinks (destroying less than 5% of the amount reacting with CO and CH<sub>4</sub>), and are not analyzed further here.

Water vapor concentrations were calculated from hourly average measurements of relative humidity obtained from the Summit meteorological station (K. Steffen, Univ. Colorado, personal communication, 2001). CH<sub>3</sub>CHO was estimated from HCHO measurements, using an estimated [CH<sub>3</sub>CHO]:[HCHO] ratio of 0.5, based on measurements at Alert (P. Shepson, pers. commun., 2000; see also Grannas et al., 2002). CH<sub>3</sub>OOH was set equal to the measured H<sub>2</sub>O<sub>2</sub>, based on previous measurements in Antarctica (Riedel et al., 2000). H<sub>2</sub> was set at a mixing ratio of 500 ppbv (Warneck, 2000).

## 2.2. Photodissociation rate constants

Photolysis rate constants were calculated using a radiative transfer model constrained by the measured downwelling component of *J*<sub>NO<sub>2</sub></sub>. The Phodis radiative transfer model, Version 0.40 (Kylling et al., 1995) was

used in six-stream, pseudo-spherical mode, assuming clear-sky conditions, using a standard subarctic summer atmosphere, and without addition of aerosol. Surface albedo was set to 0.95, based on previous analyses of the albedo of clean snow in the ultraviolet (Warren, 1982; Junkermann, 1994; Dickerson et al., 1982). The overhead ozone column was obtained from TOMS measurements, and varied daily. Absorption cross sections and quantum yields recommended by DeMore et al. (1997) were used, with the exception of acetaldehyde, for which we used the recommendations of Atkinson (1994), and  $O_3$ , for which the updated quantum yield was used (Sander et al., 2000).

Calculated  $J$ -values for all compounds were corrected for the effects of clouds using a comparison of measured and modeled  $J_{NO_2}$ . (This method implicitly assumes that the effect of clouds is independent of wavelength, which it is not (e.g. Kylling et al., 1997). However, the potential error introduced by this assumption is judged to be small relative to other sources of uncertainty in the steady-state analyses.) The downwelling component of the  $NO_2$  photodissociation rate constant was determined with a  $2\pi$  Metcon filterradiometer. Radiometer sensitivity was referenced to the manufacturer's transfer standard and temperature correction was applied to account for temperature dependence of the  $NO_2$  absorption cross section and quantum yield (Volz-Thomas et al., 1996). During clear-sky periods, the measured and modeled  $J_{NO_2}$  values differed by a nearly constant ratio, with average measured/modeled equal to 0.820, similar to the findings of Simpson et al. (2002) using the same filterradiometer during the ALERT 2000 study. All measured values were adjusted by the factor of 0.820 to agree with the model results. The effect of clouds was then taken into account by multiplying all model-calculated photodissociation rate constants by the ratio of  $J_{NO_2}$  (adjusted measurements)/ $J_{NO_2}$  (model), at each measurement time.

### 3. Results and discussion

A summary of the main parameters used in the  $PO_2$  and OH calculations is provided in Table 2. The required simultaneous measurements were available most frequently during the late morning to late evening period. During late night and early morning, insufficient data were obtained for adequate precision of average estimated concentrations. Missing measurements entirely precluded calculations for times before 05:00 (1999 and 2000) or after 20:00 (1999) or 21:00 (2000). The two seasons differed significantly in the levels of many compounds, especially HCHO,  $H_2O_2$ , and HONO; the cause of these differences is unknown. Conditions during 2000 were also calmer and sunnier (see also Honrath et al., 2002).

In the remainder of this section, we first present and discuss the estimated  $CHO_x$  ( $PO_2 + OH$ ) and OH levels, calculated using  $\alpha = [HO_2]/[PO_2] = 0.7$ . This is followed by a brief discussion of the degree to which the calculated sources and sinks of OH and  $HO_x$  balance. Finally, as the calculated concentrations are quite high, the impacts of in situ photochemistry on the budgets of  $NO_x$ , HCHO,  $H_2O_2$ , and  $O_3$ , species that are also affected by snowpack emission or deposition, are assessed.

#### 3.1. Estimated peroxy radicals

The diurnal cycle of calculated peroxy radical mixing ratios is shown in Fig. 1. These mixing ratios, reaching average midday peaks of  $\sim 42$  and 32 pptv in 1999 and 2000, respectively, are somewhat higher than or similar to those observed at other remote regions (e.g. Hauglustaine et al., 1996; Davis et al., 1996; Penkett et al., 1997). However, this similarity is deceptive, because the sources of  $HO_x$  at Summit are significantly different from those at these other sites, which are characterized by higher water vapor concentrations and a larger radical source from ozone photolysis.

A comparison to calculated and measured peroxy radicals at Mauna Loa is instructive, because of the amount of information available from the MLOPEX studies and the fact that Mauna Loa is a surface-based site that is similar in some ways to Summit. The two sites are roughly equivalent in terms of pressure altitude (atmospheric pressure at both locations is  $690 \pm 10$  hPa), but Summit differs greatly from Mauna Loa in three respects: the presence of snow, which has a much higher albedo than the volcanic rock at Mauna Loa, its latitude, which results in larger solar zenith angles, and colder temperatures (median  $-10^\circ C$ ), which alter reaction rate constants and, more importantly, result in lower water vapor concentrations ( $< 50\%$  of those at Mauna Loa during summer). The presence of snow at Summit results in much higher sunlight intensity at longer wavelengths, and as a result midday values of  $J_{NO_2}$  calculated at Summit exceed those calculated at Mauna Loa during spring and summer (Lantz et al., 1996) by a factor of 2.4. However, at shorter wavelengths, increased  $O_3$  absorption in the longer slant light path at Summit counteracts this effect, with the result that noontime  $J_{O_3}$  values at Summit are approximately equal to those calculated at Mauna Loa during spring (Shetter et al., 1996). The combination of similar  $O_3$  photolysis rate constants and lower water vapor results in a reduced  $HO_x$  source from  $O_3$  photolysis at Summit.

Midday peroxy radical mixing ratios measured at Mauna Loa during the summertime MLOPEX 2d intensive averaged 25 pptv, while a steady-state model similar to the one used in this study predicted a value of  $\sim 38$  pptv (Cantrell et al., 1996). These values thus

Table 2  
Summary of input parameters

Parameter	1999		2000	
	Mean	Range	Mean	Range
NO (pptv) (10:00–14:00)	24.7	8.3–40.8	16.0	4.4–36.6
NO <sub>2</sub> (pptv) (10:00–14:00)	32.7	7.9–55.4	15.2	0–58.5
NO <sub>x</sub> (pptv) (full period)	49.4	2.2–90.0	39.7	0–106.
O <sub>3</sub> (ppbv)	40.5	28.4–48.7	51.9	39.9–62.8
HONO (pptv)	7.24	1.1–18.7	12.7	3.1–26.6
HCHO (ppbv)	0.74	0.03–1.9	0.12	0.058–0.20
H <sub>2</sub> O <sub>2</sub> (ppbv)	1.78	0.85–2.77	0.72	0.22–1.52
CO (ppbv)	90	—	110	92–127
CH <sub>4</sub> (ppbv)	1800	1800–1820	1816	1792–1835
H <sub>2</sub> O (% v/v)	0.40	0.17–0.60	0.29	0.13–0.50
$J_{\text{NO}_2}$ (model) (s <sup>-1</sup> )	0.015	$8.07 \times 10^{-3}$ –0.0211	0.0162	$8.00 \times 10^{-3}$ –0.0223
	0.0149	0.0155–0.0211	0.0196	0.0162–0.0223
$J_{\text{O}^1\text{D}}$ (model) (s <sup>-1</sup> )	$2.15 \times 10^{-5}$	$3.26 \times 10^{-6}$ – $4.30 \times 10^{-5}$	$2.21 \times 10^{-5}$	$2.50 \times 10^{-6}$ – $4.27 \times 10^{-5}$
	$3.23 \times 10^{-5}$	$2.44 \times 10^{-5}$ – $4.30 \times 10^{-5}$	$3.38 \times 10^{-5}$	$2.32 \times 10^{-5}$ – $4.27 \times 10^{-5}$
$J_{\text{HONO}}$ (model) (s <sup>-1</sup> )	$3.23 \times 10^{-3}$	$1.74 \times 10^{-3}$ – $4.69 \times 10^{-3}$	$3.59 \times 10^{-3}$	$1.70 \times 10^{-3}$ – $4.98 \times 10^{-3}$
	$4.21 \times 10^{-3}$	$3.44 \times 10^{-3}$ – $4.69 \times 10^{-3}$	$4.36 \times 10^{-3}$	$3.59 \times 10^{-3}$ – $4.98 \times 10^{-3}$

Ranges reflect the range of measurements used in steady-state calculations, which include the subset of all measurements that included simultaneous observations of all required species. Photolysis rate constants therefore apply to the period 05:00–20:00 for 1999, and 05:00–21:00 for 2000.

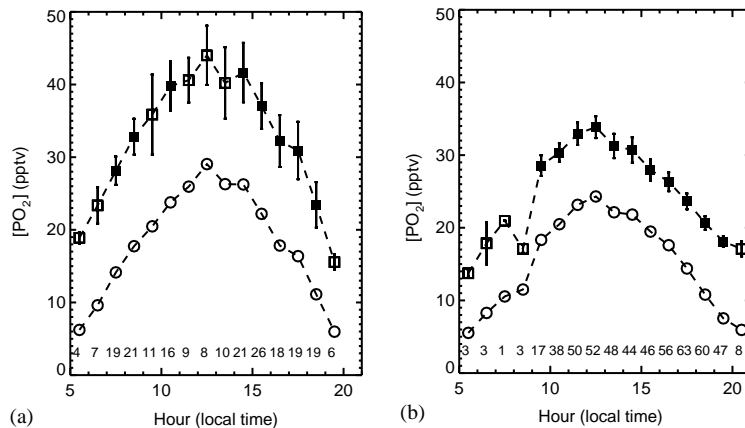


Fig. 1. The diurnal cycle of peroxy radical mixing ratio calculated using  $\text{CHO}_x$  balance with  $[\text{HO}_2]/[\text{PO}_2] = 0.7$  for (a) summer, 1999, and (b) summer, 2000. Symbols indicate the mean in each 1 h time bin; error bars extend  $\pm 2$  standard errors of the mean. The number of measurements contributing to each 1 h mean is indicated above the x-axis; means calculated from fewer than 15 measurements are indicated by open symbols. The open circles connected by dashed lines show the  $[\text{PO}_2]$  that would result if ozone photolysis were the only significant source of  $\text{HO}_x$  radicals.

approximately span the average midday peroxy radical levels calculated for Summit. However, the observed peroxy radical levels at Mauna Loa were consistent with production dominated by ozone photolysis (reactions (8) and (9)), and destruction dominated by peroxy radical recombination (Cantrell et al., 1996). Model simulations of Mauna Loa  $\text{HO}_x$  levels also indicate that  $\text{O}_3$  photolysis is the dominant  $\text{HO}_x$  source (Hauglustaine

et al., 1999), and this is generally also the case at remote marine boundary layer sites (Penkett et al., 1997). Were this the case at Summit, the combination of  $\text{O}_3$  mixing ratios and  $J_{\text{O}^1\text{D}}$  values similar to those at Mauna Loa, and significantly lower water vapor concentrations, would result in peroxy radical mixing ratios significantly lower than those observed at Mauna Loa, and significantly lower than those calculated for Summit.

This is illustrated by the dashed lines in Fig. 1, which indicate the peroxy radical mixing ratios that would balance radical production from ozone photolysis with radical destruction by reactions (15)–(17).

### 3.2. Estimated OH radical

The diurnal cycle of OH concentrations calculated by the steady-state method is shown in Fig. 2. The diurnal cycles during 1999 and 2000 differ in shape, largely as a result of the differing levels of HCHO, H<sub>2</sub>O<sub>2</sub>, and HONO noted above (see also the discussion of HO<sub>x</sub> sources, below). OH concentrations peak at  $5\text{--}8 \times 10^6$  molecules cm<sup>-3</sup>. These peak levels are similar to noontime OH concentrations during spring and summer at the somewhat similar Mauna Loa site (which, again, would be unexpected if ozone photolysis were the dominant radical source). [OH] at Mauna Loa was estimated using a steady-state model similar to that used here (Cantrell et al., 1996) and directly measured (Eisele et al., 1996): noontime simulated and measured concentrations at Mauna Loa reached  $4\text{--}6 \times 10^6$  molecules cm<sup>-3</sup> on most days. The diurnal variation of [OH] at Summit is flatter than that at Mauna Loa, however, reflecting the increased importance at Summit of photolysis of compounds more sensitive than O<sub>3</sub> to longer-wavelength actinic flux. The resulting daily average Summit OH concentration (averaged over the total period of calculations—05:00–20:00 in 1999, 05:00–21:00 in 2000—and equal to  $4.8 \times 10^6$  and  $4.5 \times 10^6$  molecules cm<sup>-3</sup> during 1999 and 2000, respectively) is significantly higher than the mean levels calculated by global models, which reach  $\sim 1 \times 10^6$  at the latitude and altitude of Summit during July (Wang et al., 1998). Indeed, it is larger than those in the tropics, the region believed to be responsible for a majority of the globally integrated OH atmospheric oxidation, due to the high OH concentrations there ( $\lesssim 3.5 \times 10^6$ ; Crutzen and

Zimmerman, 1991). (Elevated OH levels at Summit may be confined to a much smaller boundary layer, however.)

### 3.3. Sources and sinks of OH and HO<sub>x</sub>

Table 3 summarizes the total sources and sinks, integrated over 15 (1999) or 16 (2000) h, for CHO<sub>x</sub>, OH, and HO<sub>x</sub>. Since a balance of CHO<sub>x</sub> was the basis of these calculations, CHO<sub>x</sub> balances exactly. The reactions that make up the OH budget are displayed in Fig. 3; the OH budget is imbalanced, with sources exceeding sinks by 20% (1999) or 46% (2000) at  $\alpha = [\text{HO}_2]/[\text{PO}_2] = 0.7$ . This imbalance improves as the assumed value of  $\alpha$  increases, but an imbalance persists even at a value of 0.9. This suggests that an OH sink or sinks, resulting in the formation of HO<sub>2</sub> and not included in the reactions listed in Table 1, may have been present.

The budget of HO<sub>x</sub> is nearly balanced, changing from an excess of sources at  $\alpha = 0.5$  to an excess of sinks at  $\alpha = 0.7$ . The sources and sinks of HO<sub>x</sub> are shown in Fig. 4. It is here that the impact of snowpack emissions on HO<sub>x</sub> becomes most apparent. Ozone photolysis, the major source of HO<sub>x</sub> in most remote boundary-layer sites, is exceeded in importance on a daily-average basis by formaldehyde photolysis in 1999, and is equaled in importance by HONO photolysis in 2000. In both years, O<sub>3</sub> photolysis contributes <35% of the total daily-average source of HO<sub>x</sub> (calculated using the full calculation period at  $\alpha = 0.7$ ).

### 3.4. Relevance to the budgets of NO<sub>x</sub>, HONO, H<sub>2</sub>O<sub>2</sub>, and HCHO

Since the lifetime of OH is extremely short, the vertical scale over which elevated OH concentrations are present depends on the lifetimes of the precursor

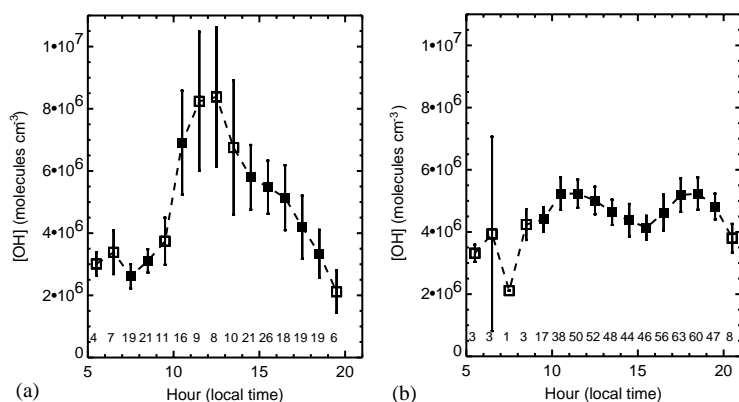
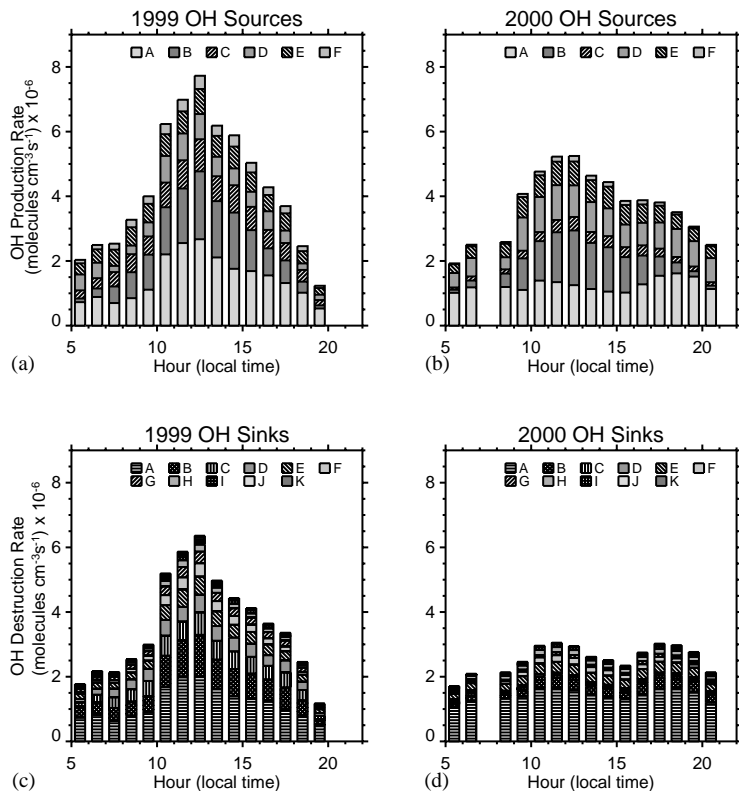


Fig. 2. The diurnal cycle of [OH] during (a) summer, 1999, and (b) summer, 2000, presented as described for Fig. 1.

**Table 3**  
Summary of radical source and sink balances

	2000			1999		
	$\alpha = 0.5$	$\alpha = 0.7$	$\alpha = 0.9$	$\alpha = 0.5$	$\alpha = 0.7$	$\alpha = 0.9$
<b>CHO<sub>x</sub></b>						
Sources	0.111	0.111	0.111	0.195	0.195	0.195
Sinks	0.111	0.111	0.111	0.195	0.195	0.195
<b>OH</b>						
Sources	0.166	0.183	0.200	0.209	0.229	0.249
Sinks	0.0994	0.125	0.151	0.152	0.190	0.228
Source/Sink	1.67	1.46	1.33	1.37	1.20	1.09
Noon [OH]	$4.0 \times 10^6$	$5.0 \times 10^6$	$6.0 \times 10^6$	$6.8 \times 10^6$	$8.4 \times 10^6$	$9.9 \times 10^6$
<b>HO<sub>x</sub></b>						
Sources	0.111	0.111	0.111	0.193	0.193	0.193
Sinks	0.0974	0.114	0.134	0.180	0.210	0.244
Source/Sink	1.14	0.97	0.83	1.07	0.92	0.79
Noon [PO <sub>2</sub> ]	38	34	32	50	44	41
Noon [HO <sub>2</sub> ]	19	24	29	25	31	37

Reaction rates reflect averages over the period of data (05:00–20:00 for 1999, and 05:00–21:00 for 2000), in units of pptv/s; [PO<sub>2</sub>] and [HO<sub>2</sub>] are displayed in units of pptv; [OH] is displayed in units of molecules cm<sup>-3</sup>.  $\alpha = [\text{HO}_2]/([\text{HO}_2] + [\text{CH}_3\text{O}_2])$ .



**Fig. 3.** The diurnal cycle of the magnitude of the most important OH sources (a and b) and sinks (c and d). Results for 1999 are shown in parts a (sources) and d (sinks); results for 2000 are shown in parts b (sources) and d (sinks). OH sources include HO<sub>2</sub> + NO (region A), O<sub>3</sub> + hv (B), H<sub>2</sub>O<sub>2</sub> + hv (C), HONO + hv (D), O<sub>2</sub> + HO<sub>2</sub> (E), and CH<sub>3</sub>OOH + hv (F). OH sinks include OH reaction with CO (region A), CH<sub>3</sub>OOH (B), HCHO (C), CH<sub>3</sub>CHO (D), CH<sub>4</sub> (E), HO<sub>2</sub> (F), H<sub>2</sub>O<sub>2</sub> (G), O<sub>3</sub> (H), H<sub>2</sub> (I), NO<sub>2</sub> (J), and NO (K).

compounds and the intensity of vertical mixing at Summit. The impact of photochemistry on the atmospheric lifetimes of  $\text{NO}_x$ ,  $\text{H}_2\text{O}_2$ , and  $\text{HCHO}$  also impacts the degree to which nitrate,  $\text{H}_2\text{O}_2$ , and  $\text{HCHO}$  ultimately incorporated into glacial ice reflect local photochemical cycling, relative to the degree they reflect the composition of the larger atmosphere. To explore these issues, we briefly discuss the photochemical sources and sinks of these compounds.

Table 4 displays the main in situ sources and sinks of  $\text{NO}_x$ , HONO,  $\text{H}_2\text{O}_2$ ,  $\text{HCHO}$ , and  $\text{O}_3$ . With the exception of HONO, rates of destruction are slow enough that these compounds are expected to mix throughout the boundary layer. The sinks of  $\text{NO}_2$  and HONO may be compared to the  $\text{NO}_x$ , HONO, and  $\text{HNO}_3$  fluxes determined using gradient measurements during summer 2000 (Honrath et al., 2002). To do this, a vertical dimension over which the calculated gas-phase rates apply is required. Helmig et al. (2002) measured midday boundary layer heights of 70–250 m during the 2000 study; the minimum height of 70 m is used here as a rough estimate of the daily averaged height over which

the reaction rates summarized in Table 4 apply, since a surface-based inversion generally developed in the late evening.

The degree to which conditions at the sampling inlets were characteristic of those throughout the 70 m mixed layer is, however, dependent on the intensity of turbulent mixing. This may have been resulted in non-homogeneous conditions in two ways. First, snowpack interstitial air concentrations of  $\text{NO}_2$  greatly exceed those of  $\text{NO}$  (Dibb et al., 2002). Emitted  $\text{NO}_2$  and  $\text{NO}$  may approach steady state as they diffuse through the snowpack, but whether this is the case is not known. The estimated characteristic times for turbulent mixing from the snow surface to the  $\text{NO}_x$  inlets at 47 and 200 cm were 22 and 68 s, respectively (median values calculated during periods when measurements were made at those heights), estimated as  $\tau_t = z/(\kappa u_*)$  (Lenschow and Delany, 1987), where  $\kappa = 0.4$  is the von Karman constant, and the friction velocity  $u_*$  was determined from eddy covariance measurements (Honrath et al., 2002). Since these values are less than the period required for approach to  $\text{NO}_2$ – $\text{NO}$  steady state, it is

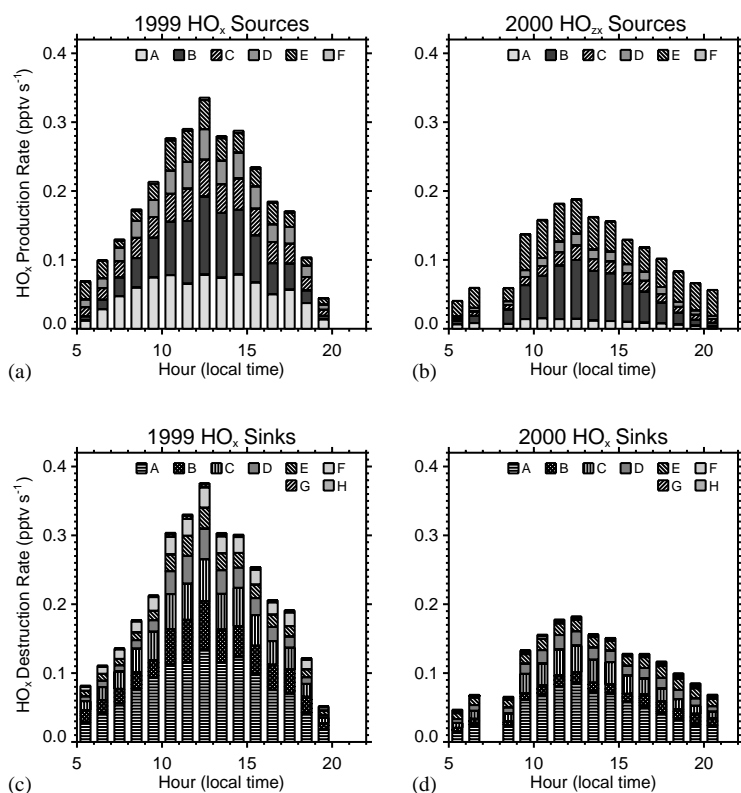


Fig. 4. The diurnal cycle of the magnitude of the most important  $\text{HO}_x$  sources (a and b) and sinks (c and d). Results for 1999 are shown in parts a (sources) and c (sinks); results for 2000 are shown in parts b (sources) and d (sinks). Sources include  $\text{HCHO} + h\nu$  (region A),  $\text{O}_3 + h\nu$  (B),  $\text{H}_2\text{O}_2 + h\nu$  (C),  $\text{CH}_3\text{OOH} + h\nu$  (D),  $\text{HONO} + h\nu$  (E), and  $\text{CH}_3\text{CHO} + h\nu$  (F).  $\text{HO}_x$  sinks include  $\text{HO}_2 + \text{HO}_2$  (region A),  $\text{OH} + \text{CH}_3\text{OOH}$  (B),  $\text{HO}_2 + \text{CH}_3\text{O}_2$  (C),  $\text{OH} + \text{HO}_2$  (D),  $\text{OH} + \text{CH}_4$  (E),  $\text{OH} + \text{CH}_3\text{CHO}$  (F),  $\text{OH} + \text{NO}_2$  (G), and  $\text{OH} + \text{NO}$  (H).

Table 4  
Impacts on the budgets of non-HO<sub>x</sub> species

Compound	Reaction	Average rate (pptv/h)			
		1999		2000	
		0500–2000	1000–1400	0500–2100	1000–1400
NO <sub>x</sub>	Sink: NO <sub>2</sub> + OH	8.6	14.6	4.4	4.4
HONO	Sink: HONO + <i>hν</i>	92.9	147.1	142.9	184.8
	Source: NO + OH	3.2	6.1	3.1	2.6
H <sub>2</sub> O <sub>2</sub>	Sink: H <sub>2</sub> O <sub>2</sub> + <i>hν</i>	56.1	82.2	21.2	32.0
	Source: HO <sub>2</sub> + HO <sub>2</sub>	144.0	215.2	86.3	138.6
HCHO	Source: OH + OH	0.02	0.03	0.01	0.01
	Sink: HCHO + OH	83.0	120.1	13.8	15.1
	Sink: HCHO + <i>hν</i>	98.8	133.4	17.3	25.2
O <sub>3</sub>	Source: CH <sub>4</sub> + OH <sup>a</sup>	< 60.4	< 97.3	< 49.0	< 58.2
	Source: NO + HO <sub>2</sub>	279.1	461.8	217.4	232.5
	Source: NO + CH <sub>3</sub> O <sub>2</sub>	115.2	190.6	90.0	96.1
	Sink: O <sub>3</sub> + <i>hν</i> (+H <sub>2</sub> O)	95.0	169.2	70.8	133.6
	Sink: O <sub>3</sub> + HO <sub>2</sub>	103.7	134.3	96.0	127.6
	Sink: O <sub>3</sub> + OH	22.9	37.6	23.7	27.8

<sup>a</sup>The rate of the reaction of CH<sub>4</sub> with OH provides an upper limit on the rate of formaldehyde formation, since most of the CH<sub>3</sub>O<sub>2</sub> radicals ultimately formed are expected to react with HO<sub>2</sub> in this low-NO<sub>x</sub> environment. (The minimum fraction forming HCHO, calculated assuming that all PO<sub>2</sub> is HO<sub>2</sub>, is approximately 13%.)

Results are shown for steady-state calculations with  $\alpha = 0.7$ .

possible that NO<sub>2</sub>/NO ratios at the sampling inlets were higher than those applicable aloft. If so, then the volume-average rate of the NO<sub>2</sub> + OH reaction shown in Table 4 would be overestimated. Second, the lifetime of HONO ( $1/J_{\text{HONO}} \geq 200$  s) is less than the period required for mixing throughout a 70 m height. This implies that the HONO sink shown in Table 4 is overestimated and further implies that the boundary-layer-average HO<sub>x</sub> source from HONO photolysis is less than that at the sampling height. (In contrast, the lifetimes of HCHO and H<sub>2</sub>O<sub>2</sub> are much longer, and those compounds are expected to mix throughout the mixed layer.)

The 05:00–20:00 average NO<sub>2</sub> destruction rate during 2000, shown in Table 4, would be balanced by a surface NO<sub>x</sub> emission of  $1.7 \times 10^{12}$  molecules m<sup>-2</sup> s<sup>-1</sup> (all surface fluxes will be specified in these units). It would also be expected to be balanced by HNO<sub>3</sub> deposition of an equivalent amount. The 24 h average gradient-based NO<sub>x</sub> flux estimate was  $2.5 \times 10^{12}$ , in relatively good agreement with this gas-phase destruction rate. However, a corresponding HNO<sub>3</sub> deposition was not observed (the average HNO<sub>3</sub> deposition flux was only  $7.2 \times 10^{11}$ ). As noted above, it is possible that the measured NO<sub>2</sub> concentrations were higher than those at steady-state; if so, then the average rate of HNO<sub>3</sub> production would be less. This comparison implies export of NO<sub>x</sub> from the Summit boundary layer. There is a much larger degree of disagreement between the average rate of HONO photolysis (equivalent to a

surface emission of  $5.3 \times 10^{13}$ ) and the gradient-based HONO emission ( $4.6 \times 10^{11}$ ). While it is likely that HONO concentrations are not constant throughout the boundary layer, as noted above, this discrepancy cannot be resolved by presuming that HONO's lifetime precludes it from mixing throughout the full height of the midday boundary layer; the measured HONO emission flux would be exceeded by photolysis in a layer shallower than the height at which HONO was measured.

Vertical fluxes of HCHO and H<sub>2</sub>O<sub>2</sub> were also measured during the 2000 season, using gradient techniques (Jacobi et al., 2002). These species are both emitted from and deposited to the snowpack. The rate of gas-phase destruction of HCHO, through a 70 m boundary layer, is equivalent to a surface emission of  $1.1 \times 10^{13}$ , a value larger than the maximum emission flux and much larger than the net daily HCHO emission. However, gas-phase production from CH<sub>4</sub> oxidation probably partially counteracts this. H<sub>2</sub>O<sub>2</sub> production exceeds H<sub>2</sub>O<sub>2</sub> destruction, with the net effect of gas-phase chemistry equivalent to a surface deposition of  $2.1 \times 10^{13}$ . This is similar in magnitude to the maximum rate of H<sub>2</sub>O<sub>2</sub> deposition, but is much greater than the net deposition averaged over the study period (Jacobi et al., 2002). Deposition of H<sub>2</sub>O<sub>2</sub> in fog may account for this discrepancy. These results indicate that gas-phase chemistry rapidly cycles HCHO and H<sub>2</sub>O<sub>2</sub> that is emitted from, and deposited to, the snowpack.

The impact of the O<sub>3</sub> production and destruction reactions summarized in Table 4 is a net ozone production of 2.6 ppbv (1999) and 1.8 ppbv (2000) during the 15- (1999) or 16-h (2000) calculation period. (If [NO<sub>2</sub>]/[NO] at the NO<sub>x</sub> inlet was greater than the steady-state value, then the actual rate of O<sub>3</sub> production would exceed this value.) Significant net O<sub>3</sub> production is not apparent in the diurnal cycle of O<sub>3</sub> measured at Summit, which is weak but implies net destruction (Helmig et al., 2002). Since photochemical O<sub>3</sub> destruction has been observed in the interstitial air of the snowpack at Summit (Peterson and Honrath, 2001), it is possible that deposition on the snow surface exceeds the in situ production.

#### 4. Summary and conclusions

Measurements of a suite of radical-source and -sink compounds during two summer seasons were used to constrain a steady-state model of radical sources and sinks at Summit, Greenland. In contrast to other remote surface measurement sites, ozone photolysis was not the dominant source of radicals. Photolysis of HCHO, HONO, and H<sub>2</sub>O<sub>2</sub> (all measured at elevated mixing ratios attributed to snowpack emissions) and CH<sub>3</sub>OOH (estimated), together increased the HO<sub>x</sub> production rate by a factor of  $\geq 3$ . The result is that midday peroxy radical levels (32–42 pptv) are comparable to those at lower latitude and altitude sites with higher water vapor concentrations, and average OH concentrations ( $> 4 \times 10^6$  molecules cm<sup>-3</sup> during the period of calculation: 05:00–20:00 or 21:00) exceed daily average levels in the tropical marine boundary layer.

The calculated photolysis rate constants and OH concentrations reveal some gaps in our understanding of photochemistry in the Summit boundary layer. The calculated HONO destruction rate greatly exceeds the HONO emission flux. Gas-phase reactions of H<sub>2</sub>O<sub>2</sub> and HCHO also imply that photochemistry in the atmospheric boundary layer plays an important role in the budgets of these species. The integrated rate of NO<sub>2</sub> + OH reaction is  $\sim 70\%$  of the measured NO<sub>x</sub> flux, and may be overestimated. This suggests that some of the emitted NO<sub>x</sub> is exported to the overlying atmosphere. A moderate rate of net O<sub>3</sub> production (2–3 ppbv/day) is calculated. This in situ production must compete against photochemical destruction in the snowpack (Peterson and Honrath, 2001) and an unusually high rate of O<sub>3</sub> deposition to the snow surface (Helmig et al., 2002). Finally, although the HO<sub>x</sub> budget was approximately balanced, that of OH was not, suggesting the presence of an unidentified OH sink which produced HO<sub>2</sub>.

These results imply that the atmospheric boundary layer in snow-covered regions is quite active photochemically, and imply rapid chemical cycling of (NO<sub>x</sub> +

HONO), HCHO, and H<sub>2</sub>O<sub>2</sub> within the boundary layer. Since concentrations of the radical precursors are significantly elevated in the interstitial air of the near-surface sunlit snowpack (Sumner and Shepson, 1999; Dibb et al., 2002), it is likely that photochemistry is even more active there. Future direct measurements of OH, HO<sub>2</sub>, and the radical precursor compounds analyzed here, made at heights ranging from within or near the snowpack surface to several tens of meters above, are needed to test the prediction of significantly elevated HO<sub>x</sub> levels and to better constrain the vertical extent over which elevated HO<sub>x</sub> is present.

#### Acknowledgements

The assistance of M. Dziobak, S. Guo and Y. Lu in the NO<sub>x</sub> measurements, helpful conversations with Bill Simpson (Univ. Alaska Fairbanks) regarding the  $J_{\text{NO}_2}$  measurements, and logistical support provided by PICO and the NY ANG are appreciated. We are grateful to the Danish Polar Board and the Greenlandic Home Rule government for granting us permission to work at Summit. This work was supported by the National Science Foundation under Grant No. 9979497.

#### References

- Atkinson, R., 1994. Gas-phase tropospheric chemistry of organic compounds. Journal of Physical Chemical Reference Data Monograph 2, 1–216.
- Bales, R.C., Losleben, M.V., McConnell, J.R., Fuhrer, K., Neftel, A., 1995. H<sub>2</sub>O<sub>2</sub> in snow, air, and open pore space in firn at Summit, Greenland. Geophysical Research Letters 22, 1261–1264.
- Blake, D.R., Rowland, F.S., 1986. World-wide increase in tropospheric methane, 1978–1983. Journal of Atmospheric Chemistry 4, 43–62.
- Cantrell, C.A., Shetter, R.E., Calvert, J.G., Eisele, F.L., Williams, E., Baumann, K., Brune, W.H., Stevens, P.S., Mather, J.H., 1997. Peroxy radicals from photostationary state deviations and steady state calculations during the tropospheric OH photochemistry experiment at Idaho Hill, Colorado, 1997. Journal of Geophysical Research 102, 369–378.
- Cantrell, C.A., Shetter, R.E., Gilpin, T.M., Calvert, J.G., 1996. Peroxy radicals measured during Mauna Loa observatory photochemistry experiment 2: the data and first analysis. Journal of Geophysical Research 101, 14643–14652.
- Crutzen, P.J., Zimmerman, P.H., 1991. The changing photochemistry of the troposphere. Tellus 43AB, 136–151.
- Davis, D., Nowack, J.B., Chen, G., Buhr, M., Arimoto, R., Hogan, A., Eisele, F., Mauldin, L., Tanner, D., Shetter, R., Lefer, B., McMurry, P., 2001. Unexpected high levels of NO measured at South Pole. Geophysical Research Letters 28, 3625–3628.

- Davis, D.D., et al., 1996. Assessment of ozone photochemistry in the western North Pacific as inferred from PEM-West, observations during the fall of 1991. *Journal of Geophysical Research* 101, 2111–2134.
- DeMore, W.B., Sander, S.P., Golden, D.M., Hampson, R.F., Kurylo, M.J., Howard, C.J., Ravishankara, A.R., Kolb, C.E., Molina, M.J., 1997. Chemical kinetics and photochemical data for use in stratospheric modeling, evaluation number 12. Technical Report JPL Publication 97-4, NASA Jet Propulsion Laboratory.
- Dibb, J.E., Arsenault, M., Peterson, M.C., Honrath, R.E., 2002. Fast nitrogen oxide photochemistry in Summit, Greenland snow. *Atmospheric Environment* 36, 2501–2511.
- Dibb, J.E., Talbot, R.W., Munger, J.W., Jacob, D.J., Fan, S.-M., 1998. Air–snow exchange of  $\text{HNO}_3$  and  $\text{NO}_y$  at Summit Greenland. *Journal of Geophysical Research* 103, 3475–3486.
- Dickerson, R.R., Stedman, D.H., Delany, A.C., 1982. Direct measurement of ozone and nitrogen dioxide photolysis rates in the troposphere. *Journal of Geophysical Research* 87, 4933–4946.
- Eisele, F.L., Tanner, D.J., Cantrell, C.A., Calvert, J.G., 1996. Measurements and steady state calculations of OH concentrations at Mauna Loa observatory. *Journal of Geophysical Research* 101, 14665–14679.
- Grannas, A.M., Shepson, P.B., Guimbaud, C., Sumner, A.L., Albert, M., Simpson, W., Dominé, F., Boudries, H., Bottenheim, J., Beine, H.J., Honrath, R., Zhou, X., 2002. A study of photochemical and physical processes affecting carbonyl compounds in the arctic atmospheric boundary layer. *Atmospheric Environment* 36, 2733–2742.
- Hauglustaine, D.A., Madronich, S., Ridley, B.A., Flocke, S.J., Cantrell, C.A., Eisele, F.L., Shetter, R.E., Tanner, D.J., Ginoux, P., Atlas, E.L., 1999. Photochemistry and budget of ozone during the Mauna Loa observatory photochemistry experiment (MLOPEX 2). *Journal of Geophysical Research* 104, 30275–30307.
- Hauglustaine, D.A., Madronich, S., Ridley, B.A., Walega, J.G., Cantrell, C.A., Shetter, R.E., Hübler, G., 1996. Observed and model-calculated photostationary state at Mauna Loa Observatory during MLOPEX 2. *Journal of Geophysical Research* 101, 14681–14696.
- Helmig, D., Boulter, J., David, D., Birks, J., Cullen, N., Steffen, K., Johnson, B.J., Oltmans, J.W., 2002. Ozone and meteorological boundary-layer conditions at Summit, Greenland, during June 3–12, 2000. *Atmospheric Environment* 36, 2595–2608.
- Honrath, R.E., Guo, S., Peterson, M.C., Dziobak, M.P., Dibb, J.E., Arsenault, M., 2000. Photochemical production of gas-phase  $\text{NO}_x$  from sunlight irradiation of ice-crystal  $\text{NO}_3^-$ . *Journal of Geophysical Research* 105, 24183–24190.
- Honrath, R.E., Lu, Y., Peterson, M.C., Dibb, J.E., Arsenault, M., et al., 2002. Vertical fluxes of  $\text{NO}_x$ , HONO, and  $\text{HNO}_3$  above the snowpack at Summit, Greenland. *Atmospheric Environment* 36, 2629–2640.
- Honrath, R.E., Peterson, M.C., Guo, S., Dibb, J.E., Shepson, P.B., Campbell, B., 1999. Evidence of  $\text{NO}_x$  production within or upon ice particles in the Greenland snowpack. *Geophysical Research Letters* 26, 695–698.
- Hurst, D.F., 1990. Seasonal variations in the latitudinal distribution of tropospheric carbon monoxide, 1986–1988. Ph.D. Thesis, University of California, Irvine.
- Jacobi, H.-W., Frey, M.M., Hutterli, M.A., Bales, R.C., Schrems, O., Cullen, N.J., Steffen, K., Koehler, C., 2002. Measurements of hydrogen peroxide and formaldehyde exchange between the atmosphere and surface snow. *Atmospheric Environment* 36, 2619–2628.
- Junkermann, W., 1994. Measurements of the  $\text{J}_{\text{O}^1\text{D}}$  actinic flux within and above stratiform clouds and above snow surfaces. *Geophysical Research Letters* 21, 793–796.
- Kylling, A., Albold, A., Seckmeyer, G., 1997. Transmittance of a cloud is wavelength-dependent in the UV-range: Physical interpretation. *Geophysical Research Letters* 24, 397–400.
- Kylling, A., Stamnes, K., Tsay, S.-C., 1995. A reliable and efficient two-stream algorithm for spherical radiative transfer: Documentation of accuracy in realistic layered media. *Journal of Atmospheric Chemistry* 21, 115–150.
- Lantz, K.O., Shetter, R.E., Cantrell, C.A., Flocke, S.J., Calvert, J.G., Madronich, S., 1996. Theoretical, actinometric, and radiometric determinations of the photolysis rate coefficient of  $\text{NO}_2$  during the Mauna Loa Observatory photochemistry experiment 2. *Journal of Geophysical Research* 101, 14613–14629.
- Lenschow, D.H., Delany, A.C., 1987. An analytic formulation for NO and  $\text{NO}_2$  flux profiles in the atmospheric surface layer. *Journal of Atmospheric Chemistry* 5, 301–309.
- Mauldin, R.L., Eisele, F.L., Tanner, D.J., Kosciuch, E., Shetter, R., Lefer, B., Hall, S.R., Nowak, J.B., Buhr, M., Chen, G., Wang, P., Davis, D., 2001. Measurements of OH,  $\text{H}_2\text{SO}_4$ , and MSA at the South Pole during ISCAT. *Geophysical Research Letters* 28, 3629–3632.
- Novelli, P.C., 1998. Distributions and recent changes of carbon monoxide in the lower troposphere. *Journal of Geophysical Research* 103, 19015–19033.
- Penkett, S.A., Monks, P.S., Carpenter, L.J., Clemitshaw, K.C., Ayers, G.P., Gillett, R.W., Galbally, I.E., Mayer, C.P., 1997. Relationships between ozone photolysis rates and peroxy radical concentrations in clean marine air over the Southern Ocean. *Journal of Geophysical Research* 102, 12805–12817.
- Peterson, M.C., Honrath, R.E., 2001. Observations of rapid photochemical destruction of ozone in snowpack interstitial air. *Geophysical Research Letters* 28, 511–514.
- Riedel, K., Weller, R., Schrems, O., König-Langlo, G., 2000. Variability of tropospheric hydroperoxides at a coastal surface site in Antarctica. *Atmospheric Environment* 34, 5225–5234.
- Ridley, B., Walega, J., Montzka, D., Grahek, F., Atlas, E., Flocke, F., Stroud, V., Deary, J., Gallant, A., Boudries, H., Bottenheim, J., Anlauf, K., Worthly, D., Sumner, A.L., Shepson, P., 2000. Is the Arctic surface layer a source and sink of  $\text{NO}_x$  in winter/spring?. *Journal of Atmospheric Chemistry* 36, 1–22.
- Sander, S.P., Friedl, R.R., DeMoore, W.B., Golden, D.M., Kurylo, M.J., Hampson, R.F., Huie, R.E., Moortgat, G.K., Ravishankara, A.R., Kolb, C.E., Molina, M.J., 2000. Chemical kinetics and photochemical data for use in stratospheric modeling: Supplement to evaluation

- 12: Update of key reactions. Technical Report JPL Publication 00-3, NASA Jet Propulsion Laboratory.
- Shetter, R.E., Cantrell, C.A., Lantz, K.O., et al., S.J.F., 1996. Actinometric and radiometric measurement and modeling of the photolysis rate coefficient of ozone to  $O(^1D)$  during Mauna Loa Observatory Photochemistry Experiment 2. *Journal of Geophysical Research* 101, 14631–14641.
- Simpson, W.R., King, M.D., Beine, H.J., Honrath, R.E., Peterson, M.C., 2002. Atmospheric photolysis rate coefficients during the Polar Sunrise Experiment ALERT 2000. Atmospheric photolysis rates during the Polar Sunrise Experiment ALERT2000 field campaign. *Atmospheric Environment* 36, 2471–2480.
- Sumner, A., Shepson, P., 1999. Snowpack production of formaldehyde and its impact on the Arctic troposphere. *Nature* 398, 230–233.
- Swanson, A.L., Blake, N.J., Blake, D.R., Rowland, F.S., Dibb, J.E., 2002. Photochemically induced production of  $CH_3Br$ ,  $CH_3I$ ,  $C_2H_5I$ , ethene, and propene within surface snow. *Atmospheric Environment* 36, 2671–2682.
- Tang, T., McConnell, J.C., 1996. Autocatalytic release of bromine from Arctic snow pack during polar sunrise. *Geophysical Research Letters* 23, 2633–2636.
- Volz-Thomas, A., Lerner, A., Pätz, H.-W., Schultz, M., McKenna, D.S., Schmitt, R., Madronich, S., Röth, E.P., 1996. Airborne measurements of the photolysis frequency of  $NO_2$ . *Journal of Geophysical Research* 101, 18613–18627.
- Wang, Y., Logan, J.A., Jacob, D.J., 1998. Global simulation of tropospheric  $O_3$ – $NO_x$ –hydrocarbon chemistry: 2. Model evaluation and global ozone budget. *Journal of Geophysical Research* 103, 10727–10756.
- Warneck, P., 2000. *Chemistry of the Natural Atmosphere*. Academic Press, New York.
- Warren, S.G., 1982. Optical properties of snow. *Reviews of Geophysics and Space Physics* 20, 67–89.
- Zanis, P., Monks, P.S., Schuepbach, E., Penkett, S.A., 1999. On the relationship of  $HO_2 + RO_2$  with  $j(O^1D)$  during the Free Tropospheric Experiment (FREETEX '96) at the Jungfraujoch Observatory (3590 m above sea level) in the Swiss Alps. *Journal of Geophysical Research* 104, 26913–26925.
- Zhou, X., Beine, H.J., Honrath, R.E., Fuentes, J.D., Simpson, W., Shepson, P.B., Bottenheim, J.W., 2001. Snowpack photochemical production of HONO: a major source of OH in the Arctic boundary layer in springtime. *Geophysical Research Letters* 28, 4087–4090.